Modeling the Role of Bacteria in Leaching of Low-Grade Ores

Kareem I. Batarseh and Alfred H. Stiller
Dept. of Chemical Engineering, West Virginia University, Morgantown, WV 26506

A robustious structural model is developed to describe the role of bacteria in the leaching process of low-grade ores under conditions controlled by intraparticle diffusion. The main impetus behind developing this model is to provide an insight into such systems, together with a suitable framework for interpreting experimental data. The model is derived in detail with respect to reaction chemistry and the role of bacteria in catalyzing these reactions, specifically the synergism of chemistry, physics and biology in determining the overall behavior of the system. The model is used to simulate the atmospheric oxidation of iron disulfide contained in porous solids in the presence of Thiobacillus ferrooxidans (T. ferrooxidans). The experimental data are predicted well by the model, which demonstrates its applicability and supports the view that the rate of intraparticle diffusion is the controlling mechanism for this system.

Introduction

During the past two decades there has been a growing interest among scientists to understand the bacterial role in leaching of low-grade metal ores. The contribution of microbiological activity to the degradation of sulfide minerals has been unequivocally demonstrated (Colmer and Hinkle, 1947). Examples are the chemoautotrophic, acidophilic *Thiobacillus ferrooxidans* and *thiooxidans* which have been used extensively for the biological leaching of copper, gold, and uranium. Bacterial leaching, although a series of chemical reactions, is physiological and is usually much more rapid than straightforward chemical leaching due to the catalytic role played by the bacteria which is a consequence of their mode of metabolism. This metabolism involves the oxidation of a suitable substrate and is carried out at the expense of certain nutrients taken into the bacteria in support of growth. For example, the biological extraction of iron-containing mineral sulfides involves the oxidation of ferrous to ferric as the energy source through a series of reactions; thus, this results in metal ions being released into solutions from insoluble minerals and their recovery as pure metals. The significance of bacterial leaching processes has resulted in a large number of studies in which bacterial leaching of a wide variety of minerals has been experimentally examined. Excellent reviews related to this area which emphasize the potential future revolutionary changes bacteria could have on the mining of metallic minerals are given by Dutrizac and MacDonald (1974), Brierley (1978), and Kelly et al. (1979).

Although an enormous amount of work has been conducted in the application of bacteria in the area of biohydrometallurgy, understanding the role of microorganisms in the leaching of mineral ores may, at best, be described as incomplete. This is due to the complexity of the problem since it involves an intricate interaction, a synergism, between kinetic and thermodynamic aspects of physics, chemistry, and biology. It might also be pointed out that since bacteria catalyze reactions by ion diffusion through their cell membrane, this might imply that they cannot catalyze heterogeneous reactions, that is, reactions that directly oxidize a solid material. In addition, the reactant solid usually becomes coated by solid products as a result of reactions which impose additional constraints upon diffusional phenomena. Furthermore, it has been shown that minerals near the surface are reacted before minerals deeper within the particles. Moreover, there is still a dearth of information reported in the literature regarding quantification of the mechanism(s) that control the rate of leaching.

Recently, attention has been focused on the development of mathematical models to describe these heterogeneous microbial reactions. The distinguishing feature of microbial oxi-

Correspondence concerning this article should be addressed to A. H. Stiller.

dation which causes difficulties in modeling is that the solid product formed by the reaction of the mineral with the gas is solubilized indirectly through the action of the microorganisms. Also, under the influence of bacteria, ionic products can diffuse and react with the solid; thus, resulting in further consumption of the reactant solid. All of these processes (solubilization, chemical, and biological reactions) are essential to support the life of these microorganisms. The continuous solubilization of the product as well as the biochemical reactions lead first to a gradual clearing of the pores, and then complete physical opening of the pores. Also, it might be pointed out that precipitation could occur as well. Consequently, this results in a continuous change of the pore structure. Since the pore structure is changing with time and position, causing alterations in the particles' porosities, the concomitant change in the effective diffusivity is significant, and such changes will eventually lead to variations in diffusion rates of gases and ionic species. Therefore, the correct description of such a process has to account for the change with time of properties intimately related to the pore structure such as porosity and transport coefficients. Thus, in order to properly evaluate any leaching process, it is necessary to fully understand the mass transport phenomena occurring on a small-scale system and to predict accurately reaction time-conversion relationship.

The state of the art in modeling of heterogeneous reactions in which the solid undergoes structural changes, in particular, pore plugging without any consideration of bioreactions, has been treated extensively in the literature and plethoric models were documented (for example, Szekely and Evans, 1969, 1971; Szekely et al., 1973; Ramachandran and Smith, 1977a,b; Georgakis et al., 1979; Ranade and Harrison, 1979). A common feature of all of these models is that the product occupies a larger volume than the reactant consumed, which causes the solid porosity to gradually decrease with consumption. Both distributed- and random-pore models were developed to describe in detail structural characteristics exclusively.

Refined random pore models for a distributed pore system were developed by Bhatia and Perlmutter (1980, 1981) and Bhatia (1985) who allowed for arbitrary pore-size distributions in the reacting solid and the effects of pore overlapping at higher levels of conversion. The model developed by Bhatia and Perlmutter (1980) was later used by Fortini and Perlmutter (1989) to interpret data obtained on the reductions of hematite to magnetite and of magnetite to iron under hydrogen-nitrogen-water vapor environment. Model predictions were in excellent agreement with experimental data. Recent models have extended the previous ones to account, for example, for reactions with nonuniform distribution of solid reactant (for example, Prasannan et al., 1985; Dassori et al., 1988). Also, in an attempt to unify the dichotomy among heterogeneous reaction models, Bhatia (1991) developed a general model which combines the shrinking-core approach with the internal and external surface reaction approach. Perturbation solutions for the model showed that for solids with low initial permeability, the shrinking core is always accompanied by a narrow internal reaction zone. For more details see the above reference.

The majority of the studies related to the modeling of leaching processes found in the literature are based on specimens of the desired metal to be leached. The analyses of such models are based on the shrinking-core model for the description of the biooxidation, and consequently the leaching process (for example, Cathles and Apps, 1975; Murr, 1980; Blancarte-Zurita et al., 1986; Kargi, 1989). Although a single or a combination of controlling mechanisms were assumed in the mathematical formulation, it appears that none of them has the capability in giving a complete and adequate description of the process. The most serious drawback of the above models is the assumption that the solid matrix within which the metal is embedded does not have any limitations on the transport of reactants and products. Also, these models neglect any structural changes that the internal solid is undergoing. Since these reactions occur on the interior surface rather than on the exterior surface of the solid, and since the product deposition and consumption patterns are functions of both time and position, one needs to fundamentally account for these effects. Thus, remodeling is necessarily *ad hoc*.

The purpose of this work is to fill out the above lacunas by presenting an extension of a model derived previously by Batarseh et al. (1989) to incorporate the effects of heterogeneous microbial gas-solid reactions which eventually can be used for describing leaching processes or any other similar phenomena. Another purpose is to describe its application to the oxidation of pyrite in the presence of *T. ferrooxidans*. Our objective is precise since we will quantify the mechanism that controls pyrite oxidation under the existing conditions, that is, the superimposed diffusional and kinetical contributions to the overall rate of oxidation will be determined individually.

While the ability of *T. ferrooxidans* to dissolve pyrite is a desirable reaction from a hydrometallurgical perspective, it is a persistent problem from an environmental viewpoint since it is responsible for the production of acid from mine wastes by the same exact hydrometallurgical mechanistic steps. The bacterial dissolution of pyritic material produces acidic ferrous sulfate which may cause serious acid mine drainage pollution problems. Within this framework, the rate of pyrite oxidation can be regarded as a direct measure of how much acid is produced. This is another reason why we decided to choose this system to test the applicability of the model.

In this article, the general formulations that describe the chemical reactions, conservations of individual species, and the assumptions imposed will be presented first. Following this, a detailed description of the experimental technique and comparison of measurements and predictions will be given.

Development of the Model

Let us consider a spherical particle of a low-grade ore of iron containing a distribution of small grains of iron disulfide, B, held together by a porous inert matrix. The surface of this particle is coated by an acidic, aqueous slime containing *T. ferrooxidans* capable of oxidizing ferrous to ferric ($Q_r \rightarrow Q_o$), but large enough so that it cannot penetrate the particle to get to the grains. Oxygen, A, diffuses through the bacterial film and the pores and reacts with iron disulfide grains to produce ferrous sulfate, C, bisulfate, S, and acid, H, according to (Singer and Stumm, 1970):

$$FeS_{2(s)} + 7/2\ O_{2(g)} + H_2O_{(l)} \rightarrow FeSO_{4(s)} + HSO^-_{4(aq)} + H^+_{(aq)} \quad (1)$$

Further consumptions of oxygen and iron disulfide are ob-

served through the dissolution of ferrous sulfate which has the following form:

$$FeSO_{4(s)} + H^{+}_{(aq)} \rightarrow Fe^{+2}_{(aq)} + HSO^{-}_{4(aq)} \quad (2)$$

$$Fe^{+2}_{(aq)} + 1/4\ O_{2(g)} + H^{+}_{(aq)} \xrightarrow{\text{bacteria}} Fe^{+3}_{(aq)} + 1/2H_2O_{(l)} \quad (3)$$

$$FeS_{2(s)} + 14Fe^{+3}_{(aq)} + 8H_2O_{(l)} \rightarrow FeSO_{4(s)} + 14Fe^{+2}_{(aq)} + HSO^{-}_{4(aq)} + 15H^{+}_{(aq)} \quad (4)$$

The physicochemical phenomena that are involved in the present development can be described by the following. The scenario starts with oxygen leaving the gas phase by dissolving in the bacterial film which has a thickness of δ_b. Some of the oxygen dissolved will react with the bacteria, Eq. 3, provided that Fe^{+2} is present and the remaining will diffuse through both the pores of the particle and a stagnant film of thickness δ present at the surface of the grains where it reacts with iron disulfide according to Eq. 1. As time passes, a progressively thicker solid product layer of ferrous sulfate which covers the reaction surface will be formed in which oxygen and ferric iron must diffuse to react with unreacted solid according to Eqs. 1 and 4, respectively. At any time, therefore, the grains are characterized by two receding surfaces, a reacted shell of product and an unreacted core of fresh iron disulfide which shrinks as the reactions proceed. Once such a layer is formed, it will be solubilized and Fe^{+2} will diffuse outwardly through the inert porous matrix to the slime, where it will be biologically oxidized thereby generating ferric lixiviant for reaction 4. Finally, the oxidized cation, Fe^{+3}, which the bacteria produce can then diffuse inwardly to contact the core and disappear by a redox step according to Eq. 4 which further breaks down the grains. Hence, the bacteria ensure that Fe^{+2} is oxidized back to Fe^{+3} to maintain a more or less constant supply of chemical oxidants for iron leaching which in turn can increase iron disulfide oxidation substantially. As a result, the total grain size (core plus product layer) will be reduced and/or expanded if dissolution or precipitation occurs as time progresses. Consequently, the structural pores of the inert solid matrix will open and/or close as a function of position and time due to these physicochemical changes that the reacting solid is undergoing.

As before, we will assume that the grains present at the surface of the particle are more accessible to both oxygen and ferric iron than the ones embedded within. We will follow the model development given by the prior article (Batarseh et al., 1989) except we will account for bacterial effects which will eventually result in variation of the structural matrix of the inert solid. In the development of this model, the following principal assumptions are imposed: (i) isothermal conditions prevail; (ii) the effect of external film mass-transfer resistance is negligible; (iii) particle size and shape are constants; (iv) ferrous iron and acid react with oxygen microbially on the surface of the particles (thus, no microbial growth occurs within the pores); (v) spherical symmetry of grains for all times; (vi) the chemical reactions are assumed to be rapid, so that the governing resistances are those of intraparticle and product layer diffusions; (vii) the pseudo-steady-state approximation is valid for describing the concentrations of oxygen and ferric iron; (viii) the only significant concentration gradient of reactant gas exists within the particle itself; (ix) water is always present in excess and hence it will not be included in the formulation which follows; (x) the diffusion coefficients of all species within the ash-layer and the film are independent of spatial coordinates and time and also ferrous sulfate has a constant-small void fraction; and finally (xi) local equilibrium on the surface of ferrous sulfate is maintained at any time.

Some of the above assumptions deserve a more careful justification. In general, the size of the particle remains unchanged during the course of the reaction provided that the inert material constitutes a major part of it; for example, the average grade of copper sulfide minerals in porphyry deposits is about 15.0% by weight. The pseudo-steady-state assumption, that is, that the unreacted core is stationary is discussed by Bischoff (1963, 1965), Bowen (1965), Theofanous and Lim (1971), and Krishnamurthy and Shah (1979) for both infinite and finite reaction rates. Bischoff (1963) concluded that the pseudo-steady-state assumption is reasonable for gases where the concentration of reactant in the fluid, C_A, is about 1×10^{-3} times the density of the solid, ρ_B. He also showed in a following article (Bischoff, 1965) that a perturbation solution in the parameter C_A/ρ_B, for $C_A \ll \rho_B$, is then appropriate. Krishnamurthy and Shah (1979) showed that for gas-solid systems the pseudo-steady-state approximation is always valid, while for liquid-solid systems this assumption is only valid in the case of diffusion controlled kinetics, that is, reactions are instantaneous. Thus, this assumption seems very reasonable in the present work for both oxygen and ferric iron since all the chemical reactions are assumed to be rapid.

The assumption regarding the void fraction of the ash layer to be small and remain unchanged during dissolution or precipitation produces a tremendous mathematical simplification. This assumption restricts any dissolution or precipitation to take place within the pores of the solid product, constant void fraction, which tends to underestimate the amount of solid dissolved or precipitated. Hence, only the material at the outer surface will be changed. We could remove this assumption and solve an extremely complicated problem which requires a tremendous computational time. Fancy algebraic equations as well as numerical solutions seem premature at the present. Accordingly, we will impose this assumption on the current theory and postpone improvements until we have some experimental data with which to compare model predictions. For the case of a porous solid dissolution, many past studies have investigated this phenomenon. For example, Cussler and Featherstone (1981), Cussler (1982), and Cussler et al. (1983) showed that dissolution at the surface of such solids can lead to both precipitation and dissolution in different regions within the solid. Later, Kopinsky et al. (1988) extended the above work and examined a system with one dissolution front from a finite-rate perspective and also relaxed some of the assumptions made in the previous studies. More elaborative models have been derived by Lichtner et al. (1986a,b) and Novak et al. (1989). For more details, a review of the above articles is strongly recommended.

The last assumption reduces substantially the number of independent variables needed to describe this system. A constitutive relation specifying the instantaneous local aqueous species concentrations at the solid surface requires *a priori* knowledge of the mechanism of the reaction, which is very difficult to determine in practice. Alternatively, when local

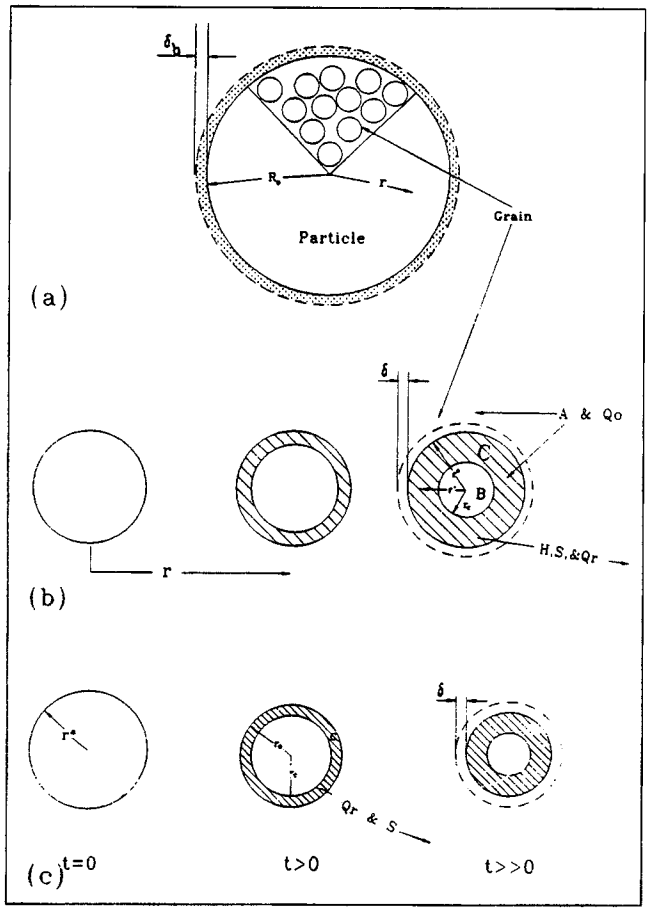

Figure 1. The model.

(a) Initial conditions; (b) development of the reaction zone as a function of radial position; (c) shrinking grain size during the course of chemical reactions as a function of time.

equilibrium between the solid phase and aqueous species is assumed, the description of the system is greatly simplified since no detailed knowledge of the reaction mechanism is needed. In this case, the rate of dissolution or precipitation can be determined at a given point in space by the change in concentration of each aqueous species with time and the local mass flux.

An important point regarding the local equilibrium approximation merits special mention: this assumption must be welcomed with trepidation, for it is only valid provided that the dissolution reaction occurs much faster than the rate of diffusional mass transport of any solute species away from the dissolving front. Within this descriptive framework, the reaction can be considered to be instantaneous and equilibrium is rapidly achieved. Accordingly, the concentrations of the solute species at the moving front are related by the pertinent equilibria of reaction 2.

The above assumptions represent adequately many processes in a number of cases. However, modifications can be made on the present model if it is necessary and are possible for some cases if these assumptions are not entirely applicable.

The model described above is sketched in Figure 1. Here, we denote by r the distance from the center of the particle (macroscopic radial coordinate), and r' the distance from the center of the grains (microscopic radial coordinate). Figure 1a is showing a section of a porous solid particle of radius R_o composed initially of uniformly sized nonporous spherical grains of iron disulfide, B. The surface of this particle is covered by a film of *T. ferrooxidans* designated by dots (.) of thickness δ_b which consume the products of the chemical reactions, ferrous iron, Q_r, and acid, H.

Figure 1b depicts the grains that constitute the solid reactant as the reaction proceeds with the unreacted core radius, r_c, decreasing monotonically from its initial radius value, r^*, while forming an ash layer of ferrous sulfate, C. It shows a row of grains that have undergone a progressively lesser extent of reaction as the front proceeds toward the center of the particle. Also shown is the fluid film of thickness δ which encloses the outer surface of the grains.

A representation of grain size variation as a function of time is shown in Figure 1c for the dissolution case, where r_o represents the radius of the ash layer at any given time and position. The change in grain size (core plus ash layer) is due to the chemical and biological reactions which will result in core and ash-layer depletion, respectively. This as a result will produce structural variations in the internal solid matrix.

In what follows, the heterogeneous reaction model with a moving boundary developed by Batarseh et al. (1989) is further extended to account for structural changes as a result of microbial effects, and to use it to simulate the bacteriological leaching of iron by *T. ferrooxidans*. The objective in developing this model is to provide guidelines for the asymptotic behavior of such systems, together with a suitable framework for the interpretation of actual experimental data. At this time, the modeling is restricted to one aspect of the leaching process, which is the role played by the bacteria in such systems. One of our future goals is the extension of the model derived in this article to incorporate the leaching phenomenon.

Formulation of the Model

Since detailed derivations of the model are available elsewhere (Batarseh, 1992), we will only present the final system of equations to be solved. The symbols that appear in the following equations are defined at the end of the article.

Overall rate equations

For convenience and broader application, the principal equations are expressed in terms of dimensionless parameters as follows:

(1) For the macroscopic diffusion of oxygen:

$$\frac{1}{Z^2}\frac{\partial}{\partial Z}\left(Z^2\overline{D}_{Ae}(Z,t)\,\frac{\partial G_A(Z,t)}{\partial Z}\right)=\frac{\varphi}{\pi_A}\,V(Z,t)\,(\beta V(Z,t)+1)\times G_A(Z,t)\left[\frac{1}{1+\eta_A\left(\dfrac{V(Z,t)}{Y(Z,t)}-1\right)(\beta V(Z,t)+1)}\right] \quad (5)$$

Boundary conditions:

$$\forall t>0 \text{ at } Z=0 \quad : \quad \partial G_A(0,t)/\partial Z=0 \text{ and} \quad (6)$$

$$\forall t>0 \text{ at } Z=1.0 \quad : \quad G_A(1,t)=1.0 \quad (7)$$

Replacing subscript A by Q_o we obtain an analogous equation for the macroscopic diffusion of ferric iron:

$$\frac{1}{Z^2}\frac{\partial}{\partial Z}\left(Z^2\overline{D}_{Qoe}(Z,t)\frac{\partial G_{Qo}(Z,t)}{\partial Z}\right) = \frac{\varphi}{\pi_{Qo}}V(Z,t)(\beta V(Z,t)+1) \times G_{Qo}(Z,t)\left[\frac{1}{1+\eta_{Qo}\left(\frac{V(Z,t)}{Y(Z,t)}-1\right)(\beta V(Z,t)+1)}\right] \quad (8)$$

Boundary conditions:

$$\forall t>0 \text{ at } Z=0 \quad : \quad \partial G_{Qo}(0,t)/\partial Z = 0 \text{ and} \quad (9)$$

$$\forall t>0 \text{ at } Z=1.0 \quad : \quad \partial G_{Qo}(1,t)/\partial Z = -\Delta\partial G_{Qr}(1,t)/\partial Z \quad (10)$$

(2) For the macroscopic diffusion of ferrous iron:

$$\frac{\partial}{\partial t}(\epsilon(Z,t)G_{Qr}(Z,t)) = \theta_{Qr}\left\{\frac{1}{Z^2}\frac{\partial}{\partial Z}\left(Z^2\overline{D}_{Qre}(Z,t)\frac{\partial G_{Qr}(Z,t)}{\partial Z}\right) - \frac{\varphi}{\pi_{Qr}}V(Z,t)(\beta V(Z,t)+1)\cdot\left(G_{Qr}(Z,t)-\xi^o_{Qr}\right)\right\} \quad (11)$$

Initial condition:

$$0\le Z\le 1.0 \text{ at } t=0 \quad : \quad G_{Qr}(Z,0)=0 \quad (12)$$

Boundary conditions:

$$\forall t>0 \text{ at } Z=0 \quad : \quad \partial G_{Qr}(0,t)/\partial Z = 0 \text{ and} \quad (13)$$

$$\forall t>0 \text{ at } Z=1.0 \quad : \quad G_{Qr}(1,t)=0 \quad (14)$$

Equivalent formulation can be written for bisulfate by replacing Q_r by S:

$$\frac{\partial}{\partial t}(\epsilon(Z,t)G_S(Z,t)) = \theta_S\left\{\frac{1}{Z^2}\frac{\partial}{\partial Z}\left[Z^2\overline{D}_{S_e}(Z,t)\frac{\partial G_S(Z,t)}{\partial Z}\right] - \frac{\varphi}{\pi_S}V(Z,t)(\beta V(Z,t)+1)\cdot\left[(G_S(Z,t)-\xi^o_S)\right]\right\} \quad (15)$$

Initial condition:

$$0\le Z\le 1.0 \text{ at } t=0 \quad : \quad G_S = G_S^\infty \quad (16)$$

Boundary conditions:

$$\forall t>0 \text{ at } Z=0 \quad : \quad \partial G_S(0,t)/\partial Z = 0 \text{ and} \quad (17)$$

$$\forall t>0 \text{ at } Z=1.0 \quad : \quad \partial G_S(1,t)/\partial Z = 0 \quad (18)$$

(3) The effective diffusivity is given by:

$$\overline{D}_{pe}(Z,t) = [\epsilon_o + \varphi\psi(1-V^3(Z,t))]^2 \quad (19)$$

where the subscript p can be replaced by A, Q_o, Q_r, S, or H. The tortuosity factor has been taken equal to $(1/\epsilon)$ in accordance with the model of Wakao and Smith (1955) (see Appendix).

(4) For the advancement of the reaction front:

$$\frac{Y^2(Z,t)}{V(Z,t)[\beta V(Z,t)+1]}\frac{\partial Y(Z,t)}{\partial t} = -\sigma\left[\frac{G_A(Z,t)}{1+\eta_A\left[\frac{V(Z,t)}{Y(Z,t)}-1\right](\beta V(Z,t)+1)} + \frac{\omega_{\bar{b}}G_{Qo}(Z,t)\cdot(1/\alpha'_{AQo})}{1+\eta_{Qo}\left[\frac{V(Z,t)}{Y(Z,t)}-1\right](\beta V(Z,t)+1)}\right] \quad (20)$$

Initial condition:

$$0\le Z\le 1.0 \quad \text{at } t=0 \quad : \quad Y(Z,0)=1.0 \quad (21)$$

(5) For the depletion of the ash layer:

$$\frac{\partial V(Z,t)}{\partial t} = -\lambda_{Qr}\left(\frac{1}{V(Z,t)}+\beta\right)\left[\alpha'_{Qr}(\xi^o_{Qr}(Z,t)-G_{Qr}(Z,t)) - \frac{\omega_q G_{Qo}(Z,t)}{1+\eta_{Qo}\left[\frac{V(Z,t)}{Y(Z,t)}-1\right](\beta V(Z,t)+1)}\right] \quad (22)$$

$$\frac{\partial V(Z,t)}{\partial t} = -\lambda_S\left(\frac{1}{V(Z,t)}+\beta\right)\left\{\alpha'_S(\xi^o_S(Z,t)-G_S(Z,t)) - \frac{G_{Qo}(Z,t)}{1+\eta_{Q_o}\left(\frac{V(Z,t)}{Y(Z,t)}-1\right)(\beta V(Z,t)+1)}\left[\omega_{sa}\alpha'_{AQ_o}\frac{G_A(Z,t)}{G_{Qo}(Z,t)}\left(\frac{1+\eta_{Qo}\left(\frac{V(Z,t)}{Y(Z,t)}-1\right)(\beta V(Z,t)+1)}{1+\eta_A\left(\frac{V(Z,t)}{Y(Z,t)}-1\right)(\beta V(Z,t)+1)}\right)+\omega_{s'q'}\right]\right\} \quad (23)$$

Initial condition:

$$0\le Z\le 1.0 \quad \text{at } t=0 \quad : \quad V(Z,t)=1.0 \text{ and} \quad (24)$$

$$[\xi^o_{Qr}]^q[\xi^o_S]^s[\xi^o_H]^{-h''} = \Omega \quad (25)$$

Although Eqs. 5-25 are valid throughout the domain $0\le Z\le 1.0$, once $Y(Z,t)=0$ and $V(Z,t)=0$ anywhere in the particle the above system of equations has to be modified. The former condition ($Y=0$) holds whenever the grains in that

region are completely reacted, while the latter ($V=0$) holds whenever the ash layer is completely dissolved. In the proceeding analysis, the necessary equations will be derived to account for these complications. We shall first consider the case when $Y(Z,t)=0$, and afterwards solutions are developed for $V(Z,t)=0$.

To facilitate the derivation, we adopt the following physical description of the system under investigation. Let us first define Γ_g as the time required for complete conversion of the grains present at the surface of the particle. Now for times greater than Γ_g, there exist two regions within a particle which are separated by a planar moving interface denoted by $Z_g^*(t)$ that moves inward as time progresses. We refer to these regions as I_g and II_g. Region I_g represents the domain from the surface of the particle to the moving boundary, $Z_g^* \le Z \le 1.0$, where the grains have finished reacting ($Y=0$), while region II_g represents the domain from the moving boundary to the center of the particle, $0 \le Z \le Z_g^*$, where the grains are at the stage of reaction ($Y \neq 0$).

Therefore for $t<\Gamma_g$, Eqs. 5-25 are valid throughout the particle; however, for $t>\Gamma_g$ one is led to consider the position of the moving boundary since the solution depends explicitly on $Z_g^*(t)$, which is not known at this point. We therefore continue to derive the equations needed to determine this unknown moving boundary along with the equation needed to obtain the conversion of the solid reactant.

For the case of complete conversion of the grains in the particle, that is, region I_g, Eqs. 5 and 8, can be written for the case of $Y=0$ as:

$$\forall t>\Gamma_g \text{ at } Z_g^*<Z<1.0 \quad : \quad \left\{\frac{\partial}{\partial Z}\left[Z^2\overline{D}_{ie}(Z,t)\,\frac{\partial G_{ilg}(Z,t)}{\partial Z}\right]=0 \right. \tag{26}$$

Equation 26 for $i=A$ or Q_o as well as Eqs. 11 and 15 are subjected to the following boundary conditions:

$\forall t>\Gamma_g$ at $Z=1.0$:

$$\begin{cases} G_{Alg}(1,t) = 1.0 & (27a) \\ \partial G_{Qolg}(1,t)/\partial Z = -\Delta \partial G_{Qr}(1,t)/\partial Z & (27b) \\ G_{Qrlg}(1,t) = 0 & (27c) \\ \partial G_{Slg}(1,t)/\partial Z = 0 & (27d) \end{cases}$$

and

$$\forall t>\Gamma_g \text{ at } Z=Z_g^*(t) \quad : \quad \left\{G_{plg}(Z_g^*,t)=G_{pIIg}(Z_g^*,t) \right. \tag{28}$$

where G_{plg}, and G_{pIIg} are the dimensionless concentrations of solute p in regions Ig and IIg, respectively. The boundary conditions given by Eq. 28 dictates that the concentrations of diffusants at the moving interface are the same from both regions.

Equation 26 may be integrated twice to obtain:

$$\forall t>\Gamma_g \text{ at } Z=Z_g^*(t) \quad : \quad \left\{G_{ilg}(Z,t)-G_{iIIg}(Z_g^*,t) = C^i\int_{Z_g^*}^{Z}\frac{1}{\overline{D}_{ie}(Z,t)}\,\frac{\partial Z}{Z^2} \right. \tag{29}$$

where C^i is an integration constant, equaling $\overline{D}_{ie}Z^2(\partial G_{ilg}/\partial Z)$ evaluated at $Z=1.0$. The above equations have to be integrated numerically for each time step because $\overline{D}_{ie}$ is the nonanalytical function of Z.

Accordingly, in region Ig where $Y=0$, one is required to solve Eqs. 11, 15, and 29. Also, Eqs. 22, 23, and 25 are valid, but one must substitute the value of zero for Y. On the other hand, in region IIg where $Y\neq 0$, one must solve Eqs. 5-25; however, Eqs. 7, 10, 14, and 18 are replaced by Eq. 28 for each diffusing species. These matching conditions must be satisfied since at the moving boundary, $Z=Z_g^*$, the concentrations of chemical species in regions Ig and IIg must be the same.

In order to find a solution for the preceding equations, one further problem remains involving the specification of an extra boundary condition at the moving interface. The specification of this additional boundary can be obtained, therefore, from the fact that the diffusing species are conserved at the moving front so that:

$$\forall t>\Gamma_g \text{ at } Z=Z_g^*(t) \quad : \quad \left\{\theta_p\left[\overline{D}_{plge}(Z_g^*,t)\,\frac{\partial G_{plg}}{\partial Z} - \overline{D}_{pIIge}(Z_g^*,t)\,\frac{\partial G_{pIIg}}{\partial Z}\right] + [G_{plg}(Z_g^*,t)-G_{pIIg}(Z_g^*,t)]\,\frac{dZ_g^*}{dt}=0 \right. \tag{30}$$

This boundary is commonly referred to as the *Stefan* condition. Problems of this sort have been extensively discussed in the literature. For example, the above equation was used by Carslaw and Jäger (1959) to deal with an analogous heat-transfer problem. Also, similar classical problems which make use of this boundary condition have been discussed by Crank (1975).

Now let us proceed further to derive the necessary equations for the case where $V(Z,t)=0$. It should be noted here that the method of solution for $V(Z,t)=0$ is so closely similar to that just described for $Y(Z,t)=0$, and hence, the derivation of these equations is straightforward. However, since the ash-layer in region Ia is completely dissolved, the effective diffusivity, $\overline{D}_{pe}$, is constant and its value can be deduced from Eq. 19 which equals $(\epsilon_o+\varphi\psi)^2$. Consequently, the resulting partial differential equations (Eqs. 5, 8, 11, and 15) can be solved analytically without excessive labor. Nonetheless, evaluation of the integral constants has to be done numerically. In region IIa the same analyses can be duplicated as in the case where $Y(Z,t)\neq 0$. It is especially notable that a condition precluding a discontinuity is satisfied for aqueous species concentrations not involved in solid precipitation or dissolution at a moving front; therefore, such species will have continuous first derivatives at a moving front.

The local conversion of the solid reactant at time t, $x(Z,t)$, and at position Z is given by:

$$x(Z,t) = 1 - Y^3(Z,t) \tag{31}$$

from which the overall conversion, $X(t)$, may be calculated by integrating over the particle:

$$X(t) = 1 - 3\int_0^1 Z^2 Y^3(Z,t)dZ \tag{32}$$

The dimensionless radius of the unreacted grain core, $Y(Z,t)$, and hence the conversion, X, can be determined as a function of time and radial coordinate, once the above equations are solved.

Equations 5-32 represent the complete mathematical statement of the problem. The solution of these equations with the appropriate initial and boundary conditions will yield the profiles of the diffusing species, and the overall conversion of the solid as functions of both time and position. These equations must be solved by means of a suitable numerical technique since they are highly nonlinear.

Numerical Solution

The resulting set of modeling equations presented earlier consists of coupled partial differential equations for the aqueous and gaseous species mole fractions, positions of two moving fronts, porosity variations with conversion, and conversion of solid along with their appropriate initial and boundary conditions. Due to the complicated nonlinear structure of these transport equations, it is fruitless to attempt to solve them analytically; hence, numerical techniques must be used. In this section, the numerical algorithm adopted to solve this system of equations will be presented.

Finite difference approximations in the space variable were utilized to replace the first and second derivatives yielding a set of k equations for k unknowns for each variable. The principal advantage of this approach is that sophisticated algorithms and computer codes are available for solving such systems efficiently with variable step sizes and control over error growth.

A computer program, LEACH, generated from the model developed here, has the ability to predict solid conversion, porosity variation, species concentration profiles, and the movement of the reacting fronts along the particle radial coordinate. LEACH is initiated by specifying the initial conditions, and other evaluated and measured parameters. Since the mathematically "stiff" nature of the differential equations can render the stability of the problem, the step size of integration was adjusted automatically by the program.

Solution procedure

The solution algorithm proceeds as follows:

(I) The physical constants and initial and boundary conditions were specified by the problem.

(II) A time of interest was selected.

(III) Equations 5 and 8 were integrated from $Z = 0$ radially outward until $Z = 1.0$ by discretizing the spatial coordinate through subdividing the volume on a fixed grid of node points with equal separation using the DEPISODE package.

(IV) Similarly, Eqs. 11, 15 and 20 were integrated in the time variable from $Z = 0$ to $Z = 1.0$ using variable-step variable-order backward differentiation method with a finite difference approximation to Jacobian.

(V) Steps III and IV produce a system of equations that was factored by a Gaussian elimination for band matrix employing LINPACK package. Matching conditions for the concentration profiles were checked using Eqs. 28 and 30.

(VI) The set of nonlinear equations, Eqs. 22, 23 and 25, were solved by a trial-and-error procedure using Newton-Raphson iteration scheme. This routine is coupled with a direct search optimization algorithm to minimize convergence difficulties caused by poor initial root guesses. The solution is as follows:

(a) Assign a value for ξ^o_{Qr}, named old ξ^o_{Qr} and calculate $\partial V/\partial t$ from Eq. 22.

(b) Calculate ξ^o_S from $\partial V/\partial t$ using Eq. 23.

(c) Calculate ξ^o_{Qr}, named new ξ^o_{Qr}, from Eq. 25.

(d) Repeat Steps a-c until new and old ξ^o_{Qr} converge.

(VII) Solution of the above steps yields local interior profiles of conversion in the particle according to Eq. 31.

(VIII) Average conversion was computed by integrating the local conversions obtained from step VII over the volume of the particle, Eq. 32, using Simpson's Rule.

Comparison with Experimental Data

Background

The purpose of this section is to give a critical examination of the literature most relevant to the present system under investigation. The major emphasis will be focused on the mechanisms of *T. ferrooxidans* on the enhancement of pyrite dissolution, in particular, the growth of this bacterium on the oxidation of ferrous iron, Fe^{+2}, by O_2 in acid medium as well as the physiological conditions under which this organism can be grown since these data are essential for calculating model parameters. Special attention is placed on the importance and the relationship among the different controlling regimes relative to the biological solubilization of FeS_2.

Physiological Aspects and Aqueous Reaction Chemistry. The iron oxidizing bacterium *T. ferrooxidans* was isolated from a coal mine drainage, and its recovery was reported by Colmer and Hinkle in 1947. Following its discovery, this microorganism was soon associated with the commercial extraction of copper and uranium from ores by microbial leaching through oxidation and acidification. *T. ferrooxidans* is a motile, single-pole flagellated, aerobic, chemoautotrophic, rod-shaped cell (0.3-0.4 μm across by 0.5-0.7 μm long), gram-negative, and its division time is variable with conditions (Brierley, 1978; Murr, 1980; Ingledew, 1982). *T. ferrooxidans*, which is a member of the thiobacilli group, is the major microorganism important in ore leaching operations, where it solubilizes, for example, sulfide minerals and produces copious amounts of sulfuric acid, releasing metal ions into leach solutions. The bacterial leaching is achieved by the ability of this microorganism to oxidize ferrous to ferric iron as the energy-generating reaction for growth. The acidic pH of the leaching media as well as the temperature of the growth environment are of critical importance. The precise optimum values reported for the pH and temperature vary and are in the range of 1.0-2.5 for the former and 20-45°C for the latter.

The ability of this organism to oxidize Fe^{+2} to Fe^{+3} provides

the energy-generating reactions for growth. This energy-generating system which resides within the cell envelope (Ingledew et al., 1977) is mediated through an electron-transport chain between two half reactions which are catalyzed by *T. ferrooxidans*. Physiologically, the following events occur: Fe^{+2} is oxidized according to:

$$Fe^{+2}_{(aq)} \xrightarrow{\text{bacteria}} Fe^{+3}_{(aq)} + \bar{e} \tag{33}$$

consequently, O_2 can be reduced to H_2O by:

$$\bar{e} + \frac{1}{4} O_{2(g)} + H^{+}_{(aq)} \xrightarrow{\text{bacteria}} \frac{1}{2} H_2O_{(l)} \tag{34}$$

where the electron transferred produces enough energy to insure the formation of ATP when coupled to oxidative phosphorylation. The sum of Eqs. 33 and 34 is given by Eq. 3. Because of the ability to oxidize Fe^{+2} to Fe^{+3}, *T. ferrooxidans* is able to solubilize pyrite.

Although iron oxidation occurs over the pH range of 1.0 to 4.5, the biogenic reaction, Eq. 3, takes place at pH values of less than 3.5. Moreover, it was concluded by Ingledew (1982) that the higher the pH the greater redox potential energy available, yet, *T. ferrooxidans* does not exploit this available energy. The reason behind it is at pH of 4.0, abiotic oxidation rates of Fe^{+2} substantially increase (Ingledew, 1982), which will lead to the production of toxic intermediates such as O_2^- and/or O_2^{-2} while substrate, Fe^{+2}, is being depleted. Also, above pH of 3.0, the precipitation of ferric iron is noticeable (Lacey and Lawson, 1970). This required acidity is provided by the production of H^+ via reactions 1 and 4.

Diffusional Limitations. Silverman et al. (1961) studied the oxidation of pyrite in the presence of *T. ferrooxidans*. They showed that pyrite was more rapidly oxidized at less than 44 than at 210 μm in Warburg respirometer experiments. Ehrlich and Fox (1967) found that reduction in particle size from 177–125 to less than 62 μm doubled the rate of bacterial oxidation of metals. The effect of particle size on the oxidation rates of minerals under the influence of *T. ferrooxidans* has been examined by Torma (1977) who found that greater oxidation rates occur when the particle size was decreased. Torma and Guay (1976) studied the parameters of specific surface area, total surface area, and particle size to obtain information regarding the biodegradation of sphalerite (ZnS) concentrate by *T. ferrooxidans*. It was found that the highest oxidation rates were obtained using the smallest size fraction with the highest exposed surface area.

Pinches et al. (1976) concluded that the most important factor affecting the rate of leaching was the size of the mineral particle when it was inoculated with *T. ferrooxidans*. They discovered that the particle reduction allowed additional metal to be solubilized. Also, they found, as did Torma and Guay (1976), that mineral yield was proportional to the external surface area for particles larger than 7 μm. It was also found that the rates of biooxidation increased linearly with decreasing particle size but are less dependent when the particle sizes were very small. They indicated that the particle-size phenomenon might be a geometrical effect, and they also suggested that smaller particle size might affect microbial/mineral interactions. The above findings emphasize that diffusion plays an important role in determining overall rate behavior of such processes.

It is apparent from the above that the availability of soluble nutrients is undoubtedly the most important factor which controls bacterial extraction of metals. The most likely rate-limiting nutrients in the present case are dissolved oxygen, hydrogen, ferrous, ferric, and bisulfate ions since they are required to sustain the necessary reactions given by reactions 1-4. The inward diffusions of O_2 and Fe^{+3} are limited by diffusion through the pore space of the particle, the stagnant film of liquid surrounding the grains, and finally diffusion through the ferrous sulfate layer formed according to reactions 1 and 4 to react with iron disulfide. The outward diffusions of H^+, Fe^{+2}, and HSO_4^- resulting from reactions 1 and 4 follow the same exact path as of O_2 or Fe^{+3}, but in the opposite direction, however, the diffusion of Fe^{+2} or HSO_4^- which results from the dissolution of $FeSO_4$ according to reaction 2 is limited by diffusion through both the stagnant film and the pores of the particle.

Experimental

The equipment and techniques used are very important and, therefore, require description. In addition, the experimental methods used to measure porosity and other pellet properties are described. Since the changes in the internal structural properties of the solid matrix that accompany the reactions are crucial to the results, this placed rather severe limitations on the procedure used to quench the chemical and biological reactions. The method adopted is described below.

Sample Preparation. Samples for these experiments were handpicked from mines in West Virginia in which all the parameters concerning pyrite content and grain size were determined in a parallel study. These samples were low-grade run-of-the-mine waste rocks which were collected from various strip mines, chosen for their availability, and contrasting physical and chemical properties. The three types of waste rocks used in this study are identified by code numbers: 0751, 1262, and 3161. Sample designations, locations of the mines, analyses for iron, and grain size are reported in Table 1.

The as-received samples were crushed by a jaw crusher, and sieved using Tyler U.S. Standard testing sieves into one discrete particle-size fraction. The fraction of particles within size ranges 0.2794–0.2362 cm ($\bar{D}_p = 0.2578$ cm) was investigated in this study. Following this, the samples were split subsequently into 60 gm portions. Some of these portions were ground to a size of 110 μm for use in the powdered isotherm studies by a Tyler screen shaker. The graded material was then washed free from ferrous iron and any other debris by leaching for a 24-hour period. This step also ensured the absence of bacteria. To

Table 1. Identification and Analysis of Pyrite for Samples Used in This Study

Sample No.	Type	Origin	% Pyrite Content* (g/g)	Grain Radius (cm)
0751	Roof Shale	Greenbrier Co.	10.5	0.00849
1262	Sandstone L	Greenbrier Co.	4.3	0.00297
3161	Sandstone D	Monongalia Co.	1.63	0.00495

*Obtained by the LECO method.

eliminate any oxidation, the prepared materials were sealed in plastic bags under nitrogen gas and stored in a cold room at 4°C until the experiments were conducted.

Structural Properties Measurements. Mercury penetration porosimetry was used to study the macropore structure of the samples. The instrument provided mercury penetration pressure up to 413.5 MPa, corresponding to a minimum measurable pore radius of 15 Å with an error of ≈1%. The true powder as well as the bulk densities needed to calculate the porosity were obtained from the same experimental technique.

Bacteriological Procedures: Microorganisms. Pure cultures of *T. ferrooxidans* (strain ATCC No. 13598) were kindly supplied by Dr. Gregory Olson of the Pittsburgh Dept. of Energy, Pittsburgh, PA. These cultures were grown by employing medium 9K of Silverman and Lundgren (1958). This medium's compositions compare favorably with the major chemical constituents of acid mine effluents. The 9K medium was adjusted to pH 2.8 with sulfuric acid.

Chemical and Instrumental Procedures. Two groups of experiments were performed in this investigation. The first group consisted of experimental techniques to obtain values for the pore structure parameters, and the second set was based on soxhlet extraction which generated conversion vs. time data for comparison with the model predictions. A particle size of $\overline{D}_P = 0.2578$ cm was selected and three temperatures: 20, 30 and 37°C were investigated.

Before inoculation, the bacteria were harvested by centrifugation at 8,000 rpm for 10 min, washed with 25 mM sulfuric acid until no mineral salts were collected, and suspended in sulfuric acid at pH = 1.3. This allowed the bacteria to be in a stage of suspension or starvation. After this, the prepared rock samples were incubated with 1.29×10^{-5} g/cm^3 of *T. ferrooxidans*, which compares favorably with bacterial concentration present in acid mine effluents. The flasks which contain the samples were inoculated at 4°C in order to halt bacterial activity. A pulp density of 120 g/mL (solid weight (g) × 100/liquid volume (mL)) was maintained throughout the inoculation period. Following this, the liquid was drained, and the contaminated rock samples were placed in a porous cellulose thimble for the initiation of the oxidation experiments.

Experiments to study bacterial leaching of pyrite within these samples have been carried out isothermally in a stationary batch reactor. The reactor consisted of a 45 × 123 mm porous cellulose thimble with the top open to the atmosphere. It was decided to investigate the kinetics of batch oxidation as it was considered that batch processes would imitate closely field conditions.

The normal procedure was to pack loosely the cellulose thimble with 60 gm of the prepared samples, and insert it into an incubator at the desired operating temperature under atmospheric oxygen environment. The activation was presumed to be initiated once the samples were in the incubator. The temperature was controlled to within ±1°C. Following this, samples were withdrawn at well-defined time intervals for chemical analyses to determine the conversion vs. time response at the given reaction conditions. To demonstrate the reproducibility of these responses, triplicate runs were performed for each sample at each operating condition in which the chemical analyses were averaged and the results were reported. Further details on the procedure are reported elsewhere (Batarseh, 1992).

Kinetic data were obtained by leaching the samples with distilled, deionized water in a soxhlet extractor for 24 h, following the detailed procedure presented by Renton et al. (1984). The resulting leachate was analyzed for iron and sulfate. Sulfate analysis was carried out by the barium sulfate turbidimetric procedure while iron concentration was determined by atomic absorption spectrophotometry with a Spectrophotometer 2380 Perkin-Elmer.

The objective of the study placed rather severe limitations on the method used to terminate the chemical and biological reactions. Conventional procedures such as chemical or ultrasonic methods turned out to be formidable tasks because destruction of the internal pore structure of the particle is unavoidable. Several approaches were suggested before a satisfactory procedure was reached. The procedure adopted was based on terminating the reactions at the desired conversion level by rapidly transferring the sample to a plastic bag filled with nitrogen and placing it into a hot oven. The thermal step was undertaken to kill the bacteria instantly, since it was suspected that *T. ferrooxidans* can utilize dissolved oxygen already present in the pores for respiration, a step which could not be avoided. After the reactions were quenched, the partially-reacted samples were submitted for analyses of physical properties and pore structural characteristics.

To ascertain the role of *T. ferrooxidans* in the acceleration of pyrite oxidation, identical uninoculated samples were also studied. These samples which were used as controlled samples were subjected to the same experimental conditions as the inoculated ones.

Preliminary Work

Each experiment, unless stated otherwise, was performed in triplicate with the analyses averaged and reported. The data was put on a comparative basis by measuring the amounts of sulfate and total iron collected in the leachates and stoichiometrically converting them to normalized weight changes of pyrite reacted. The actual oxidation studies were accompanied by extensive structural measurements; these include porosity and pore-size distribution as functions of time.

Intrinsic reactivity

In the development of the model presented here, it was assumed implicitly that the intrinsic reactivity of pyrite oxidation is independent of the rock type used. The validity of this assumption can be confirmed using the conversion profiles obtained on the powder samples. For the purpose of generality, we also examined this assumption with the sterilized samples as well. Application of statistical analyses on the variance, slope, and intercept on these profiles revealed that there is no statistically significant difference between these profiles at 95% confidence interval, indicating that the intrinsic reactivity is virtually independent of the type of rock used for both inoculated and sterilized samples (Batarseh, 1992). In the case of the sterilized samples, this observation is in accordance with a prior study conducted by the same authors. The implication of this finding is that the assumption used in the model development appears to be satisfactory.

Table 2. Physical Properties and Calculated Parameters Used in the Theoretical Predictions

			$T=$ 20°C		$T=30$°C		$T=37$°C			
		G_S^{∞}	= 122.6		145.1		163.8			
		α'_{AQ_o}	= 3.90		3.98		4.00			
		$\theta_{Qr}(d^{-1})$	= 33.1		40.3		46.6			
		$\theta_S(d^{-1})$	= 59.3		73.9		85.3			
		ξ_H^o	= 172.2		203.7		229.9			
		Ω (cm^3/mol)	= 0.749		0.886		1.00			
Sample No.	w_o (g/g)	ϵ_o	φ	ψ	$\lambda_{Qr}=\lambda_S$ (d^{-1})	σ (d^{-1})	$\lambda_{Qr}=\lambda_S$ (d^{-1})	σ (d^{-1})	$\lambda_{Qr}=\lambda_S$ (d^{-1})	σ (d^{-1})
751	0.105	0.109	24.8	1.45×10^{-3}	0.107	0.0498	0.109	0.0522	0.110	0.0536
1,262	0.0430	0.121	118.6	1.77×10^{-4}	0.874	0.406	0.893	0.426	0.900	0.436
3,161	0.0163	0.120	15.6	4.92×10^{-4}	0.312	0.146	0.322	0.153	0.331	0.157

Constants	
α'_{Qr}	$=\Delta=1.19$
α'_S	$=2.13$
β	$=2.00$
η_p	$=500.0$
π_p	$=1.00$
$\omega_{\bar{b}}$	$=0.250$
ω_q	$=1.00$
ω_{sq}	$=0.286$
$\omega_{s'q'}$	$=0.0714$

Effect of bacteria

In order to confirm the ability of *T. ferrooxidans* to enhance the oxidation of iron disulfide, experimental results for both inoculated and sterilized samples were compared for the powder, and the larger particle size (0.2578 cm) at different operating temperatures for all samples. It was found that bacteria can indeed increase the solubilization of pyrite significantly. For example, at temperature of 20°C for sample number 0751 approximately 5.70% of total pyrite was reacted within 14 days for the biotic case whereas only 1.40% was reacted for the abiotic one. This result (bacterial enhancement of mineral leaching) corroborates fully with all previous findings presented in the literature.

Rate-controlling regime

It was assumed in the development of the model that the oxidation mechanism is solely controlled by intraparticle diffusion. The validity of this assumption can be checked by the use of the following criterion. In principle, for a reaction to be diffusionally controlled, the reactivity of the powder should be appreciably greater than that of the pellets, and simultaneously temperature changes should not have significant effects on the reactivity of the pellets.

To establish the experimental conditions to determine which mechanism is controlling, the reactivities of these rock samples were measured over the temperature range of 20–37°C for two different particle sizes under both biotic and abiotic environments. It was found for both environments that reducing particle size from 0.2578 cm to 110 μm increased the subsequent overall conversion by almost five times, while at the same time temperature changes had minor effects on the conversion of the pellets (for more information see Batarseh, 1992). In the case of the abiotic environment, this observation is in accordance with our previous findings (Batarseh, 1987). These results indicate that the contributions of physical effects to the overall conversion are significant, and therefore intraparticle diffusion resistances are the ultimate controlling mechanism for this process. Apparently, the oxidation of iron disulfide proceeds rapidly on the reactive sites, but diffusions of chemical species occur slowly through both the pores of the particle and the ash layer. Since the rate is diffusion-controlled, details of chemical and intrinsic reactivity of these rocks are of no consequence. Thus, the assumption imposed appears to be opposite for the present case.

Results and Discussion

The results that follow focus on verification of the model with the aid of experimental data obtained on the biological oxidation of iron disulfide in the presence of *T. ferrooxidans*. In order to provide a common point of reference, we will compare the normalized weight changes of iron disulfide to simulation for each type of rock used. Although we have assumed isothermal conditions in the development of the mathematical model, the sensitivity of the system's behavior to temperature is also studied by comparing model predictions with actual experimental data at three different temperatures: 20, 30 and 37°C. In order to reveal the underlying structural changes, the initial as well as the developing of both porosity and pore-size distribution of the inert solid matrix were measured as functions of time, and the results are reported subsequently.

The rocks properties and basic parameter values employed in our theoretical computations are listed in Table 2. Physical properties were obtained from the literature (Perry and Chilton, 1973). The solubility of ferrous sulfate or szomolnokite in sulfuric acid (pH = 1.3), $\bar{K}_{sp}$, was determined in our laboratory and found to be 2.18×10^{-7} at 25°C. The porosity and tortuosity factor of the ash layer, ϵ' and τ', were taken to be 0.02 and 10, respectively. It is apparent that the values of ϵ' and τ' are rather low and high, respectively. This supports the premise made earlier in the development of the model regarding the void fraction of the product to be very small. By fitting

Table 3. Variations of Average Pore Diameter with Time for Inoculated Samples

Time (days)	Sample Number, $\bar{D}_r$ (μm)					
	0751		1262		3161	
	Macro	Micro	Macro	Micro	Macro	Micro
0	---	0.007	0.27	0.0058	0.80	0.006
7	---	0.0075	0.30	0.006	0.75	0.007
14	---	0.011	0.38	0.007	0.43	---
21	---	0.007	0.28	---	0.55	---
28	---	0.008	0.40	0.005	0.46	0.0062
35	0.1	0.0055	0.17	---	0.20	---

the calculated intraparticle conversion profiles to the ones obtained experimentally, the best possible correspondence for δ was found to be one-half the radius of the grain, that is, 1/2 r_o. This value falls within reasonable range—$Sh \simeq 2.0$. It is apparent that the magnitude of this parameter is a function of grain size, which is in turn a function of each individual sample. More details regarding the evaluation of some of these parameters are given in the Appendix.

Complete initial and developing pore structure for all rock samples were obtained by mercury porosimetry techniques using a Micromeritics Autopore II 9220 model. Measurements were made under both inoculated and sterilized conditions at five different reaction times: 7, 14, 21, 28 and 35 days. The results are presented in Table 3 in the form of average pore diameter with respect to reaction time. It may be noted here that only the inoculated samples' results are tabulated since the pore-size distributions for the sterilized samples were found to be virtually unaffected by the oxidation reaction, and therefore the pore structure remains intact for these samples. Table 3 clearly indicates that the biological leaching of iron disulfide had caused pronounced alterations of the pore structure, in some cases changing the pore structure entirely from a unimodal to a bimodal pore-size distribution or vice versa.

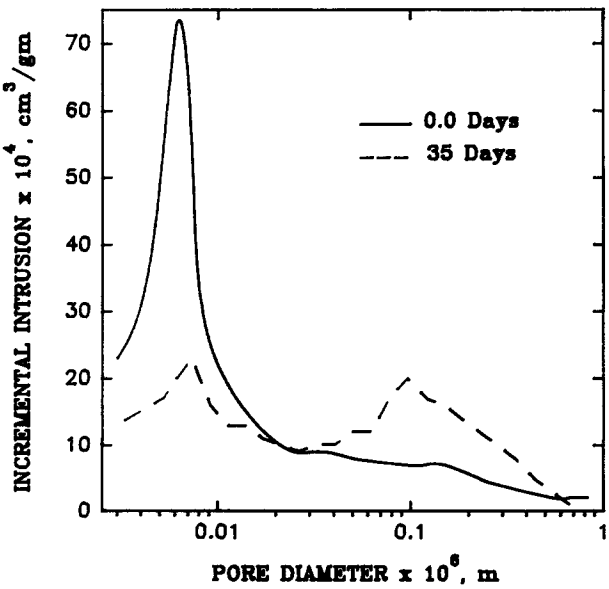

Figure 2. Variation of pore-size distribution with conversion for sample number 0751.

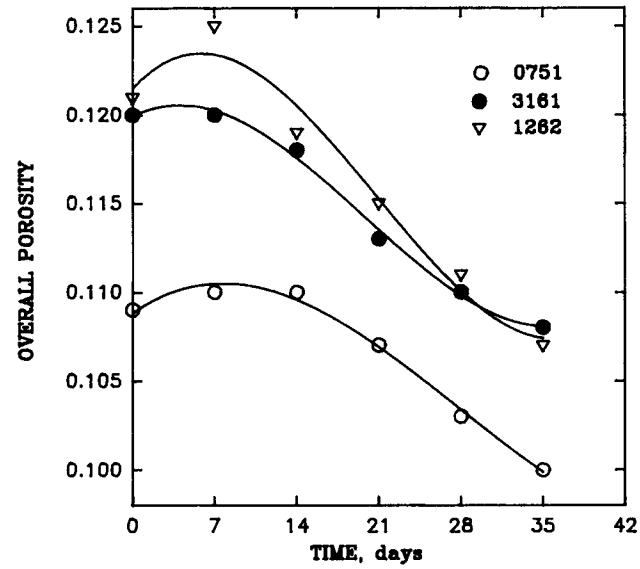

Figure 3. Variations of overall porosity with time for inoculated samples.

Figure 2, for example, shows the pore-size distribution for sample number 0751 before and after 35 days of oxidation. Initially, the pore structure is characterized by a unimodal pore-size distribution, solid line, with a mean pore diameter of approximately 0.007 μm. Biological oxidation for 35 days led to the formation of macropores, as shown by the dashed line, as well as the alteration of the original microstructure of the unreacted sample. As a result, the distribution became bimodal with average pore diameters of approximately 0.1 and 0.0055 μm for the macrostructure and microstructure, respectively. It can therefore be concluded that dissolution and precipitation of ferrous sulfate in different regions within the particle have chiefly caused the internal porous structure of the inert solid matrix to change.

Because of its direct effect on the extent of reaction rate, the porosity and its variation history with the conversion is among the most important parameters. Results obtained on the overall or global porosities are portrayed in Figure 3. For the reason stated previously, only the values obtained on the inoculated samples are shown. These data indicate that small variations in porosities are observed. Moreover, despite the dissimilarities between these rocks, a general observation holds for all of these curves shown in Figure 3 in that they are qualitatively the same. The trajectory paths of these curves go first through a maximum value at a time of approximately 7 days followed by a gradual decrease thereafter. This behavior is chiefly due to the following: At such small reaction times, the ferrous sulfate formed at the grains present near the surface of the particle will dissolve. As time progresses, however, the concentrations of both ferrous and bisulfate ions become more pronounced; consequently, this will result in a condition precluding dissolution to take place and precipitation is the norm. Thus, dissolution of ferrous sulfate encapsulating the grains has caused precipitation to take place. For this particular problem, the time required for this dissolution engendered precipitation is relatively short since the initial concentration of bisulfate ion is quite large (see Table 2).

In addition to the above, the degree to which these processes

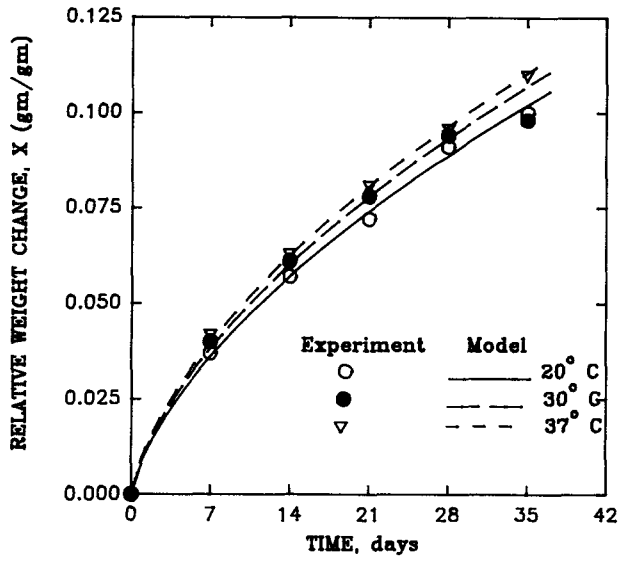

Figure 4. Comparison of experimental data with simulation for sample number 0751.

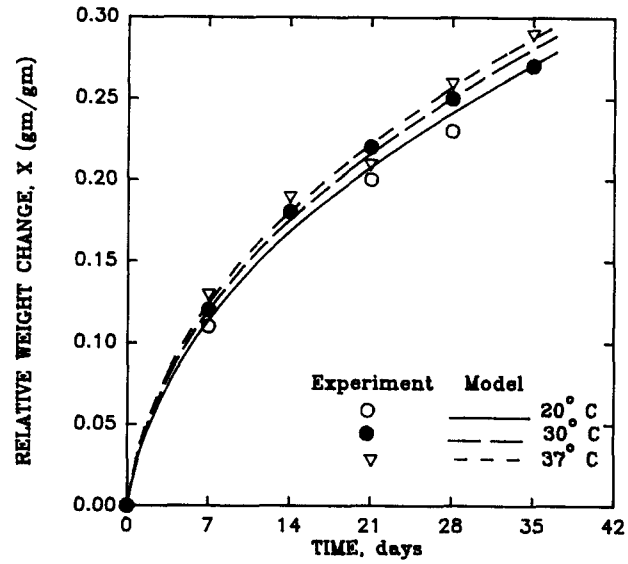

Figure 6. Comparison of experimental data with simulation for sample number 3161.

actually occur depends on the near equality of the molecular diffusion coefficients of ferrous and bisulfate since both of these ions are essentially racing among each other. In this case, bisulfate ion effectively wins the race because it has a higher molecular diffusion coefficient than that of ferrous ion. We must also keep in mind that even though these variations are relatively small, changes in local porosities are significant which in turn has direct consequences on the computer simulation results (see Eq. 19). Notice here that these values represent overall (global) porosity variations since local porosities are extremely difficult to determine in practice.

The theoretical conversion-time behavior generated by the LEACH computer program is compared to the experimental data for 0.2578 cm particles at the three operating temperatures. Such a comparison is depicted in Figures 4 through 6.

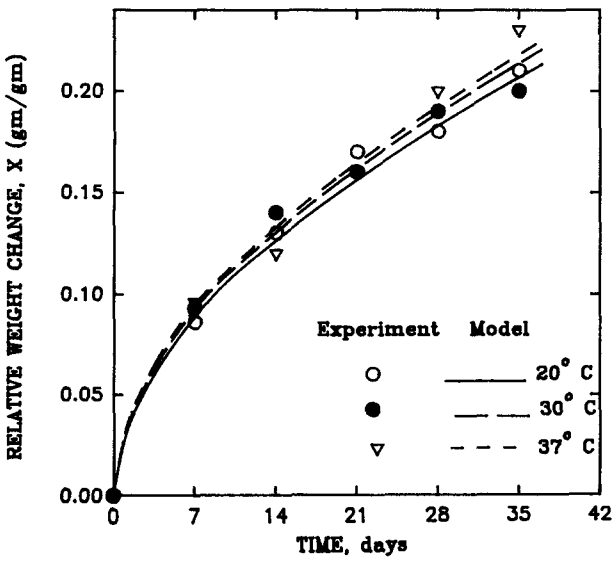

Figure 5. Comparison of experimental data with simulation for sample number 1262.

There is generally an excellent agreement between experimental data and simulation predictions. This agreement is particularly significant in that we have included rocks which differ in origin as well as physical and chemical properties. It is apparent that the salient features of the model are consistent with the response of the experimental data, including the general trend of these curves and the ultimate conversion achieved. In particular, the predicted conversion profiles are very closely associated with the experimental ones over the present temperature range. *It is crucial to note here that in all the theoretical predictions presented above the same values of* τ' *and* ϵ' *were used.*

The shape of the conversion profiles given by Figures 4 through 6 display some interesting features in that they all exhibit the same qualitative appearance. Initially, there is a sharp increase in conversion up to approximately 7 days followed by a gradual decline. This constitutes a particularly striking demonstration of the dependence of this process on intraparticle diffusion resistances which is a confirmation to what was found earlier. This can be explained by the following: As previously stated, the process is initiated by the diffusion of oxygen into the rock particle and reaction with iron disulfide with the subsequent formation of ferrous sulfate and bisulfate ion close to the surface. This is followed by dissolution of ferrous sulfate, yielding ferrous and bisulfate ions. The ferrous iron released by dissolution subsequently diffuses outward where it is consumed by the strong rates of the bacteriological reaction to form ferric iron. The ferric iron formed then diffuses inward through the particle to react with iron disulfide to produce more ferrous sulfate and ferrous iron, and the cycle is repeated. As a result, significant changes take place throughout the particle. At the initial stages of the reaction, therefore, the oxidation is solely confined to the extremely rapid reaction of oxygen with iron disulfide grains present at the surface of the particle, and thus the conversion is large in this vicinity. This behavior is represented by the high conversion of the solid reactant at small times which is an indication of the high affinity to diffusion, absence of ash-layer resistance, and sub-

sequent reaction. As time progresses, however, the accumulation of the product layer becomes significant, resulting in the associated intraparticle diffusional resistances to become more pronounced, always offsetting the oxidation process. Notice here that the dissolution of ferrous sulfate is counteracted by the continuous increase in bisulfate and ferrous ions which results in precipitation, further impeding diffusion.

The results presented here were obtained on a Hewlett-Packard mainframe Apollo Series. A simulation time of 37 days required approximately 3 h of computer time.

Conclusions

A structural intraparticle diffusion model was developed to describe the biological extraction of minerals embedded within an inert solid matrix. On the practical side, the model provides an integrated picture of the interdependence of the many facets of such processes. The model uses parameters which can be easily determined either experimentally or theoretically from already published literature data.

The model has been verified by simulating the biological oxidation of iron disulfide contained in waste rocks in the presence of *T. ferrooxidans*. Comparison of model predictions with experimental data provided excellent agreement. In particular, this comparison has served to validate quantitatively as well as qualitatively the model's features.

The model developed by this work is unique since there is a paucity of mathematical models that accounts for the significance of the bacterial/physical rock parameters interactions, viz., the importance of intraparticle diffusion is often neglected. With the presently developed model, however, it is possible to predict confidently the dynamic behavior sought in complicated problems of this nature. Accordingly, the model is extremely robust and should have a myriad of applications in a large variety of phenomena. To mention a few, the model can be used for industrial applications involving pollution problems, analogous noncatalytic gas-solid reaction systems, and many geological processes. An intriguing application of this theory is the formation of dental caries or tooth decay. Tooth decay results from the metabolism of sugars to acid by certain bacteria, *Streptococcus mutans*, that grow in a gel film called "plaque" attached to the surface of the tooth. The acid produced then diffuses to interact chemically with mineral hydroxyapatite where dissolution and precipitation can occur simultaneously. This result in demineralization of teeth and formation of dental caries.

An important point needs to be discussed concerning the numerical solution. Since the number of mesh points and time step size affect the accuracy of the results, simulations have been undertaken with different numbers of mesh points and time steps. A mesh number of 97 and a time step of 74 proved to be optimum to produce adequate accuracy. Because the particle size is small and the duration of the experiment is relatively short for our case, changes in mesh size and time step to produce accurate results can be explored economically on mainframe computer stations. However, larger particle size and longer reaction times require smaller spatial and temporal step sizes which renders the system for solution on regular computers too time-consuming; hence, supercomputers are essential. The choice of a suitable set of mesh size and time step for a specific situation is rendered by the numerical scheme in the form of unstable solution, that is, the solution does not converge. Once a stable solution is found, the mesh size and time step can be refined to obtain the necessary accuracy.

Finally, we want to sound some notes of caution. Since Knudsen diffusion does not play a role in the formulation above due to the presence of a liquid phase, interactions among the pores as well as pore growth and coalescence have negligible effects on intraparticle resistances. However, if the intraparticle mass transport process occurs in a gas phase and within the micropore or the mesopore range, a structural model which provides information regarding the structural properties of the solid as functions of local conversion is needed. Moreover, this situation may not only require solution of the pore structure evolution problem, but also a very detailed analysis of the evolving pore structure. If this is the case, then these effects can be incorporated into the present development where such changes in the internal structural properties of the solid matrix can be obtained from previously published structural models, that is, Bhatia and Perlmutter (1980, 1981), and Bhatia (1985). Indeed the inclusion of such phenomenon is a complex procedure which requires specialized software, and longer processing time; nonetheless, the model is amenable for such extensions.

Acknowledgment

The financial support of this work was provided by the Office of Surface Mining, Grant No. GR-996541.

Notation

a = stoichiometric coefficient equaling 7/2
a_P = activity coefficient of P
A = gas reactant
$\bar{b}_A$ = stoichiometric ratio equaling 2/7
$\bar{b}_{Qo}$ = stoichiometric ratio equaling 1/14
B = solid reactant
C = solid product
$C_{A\infty}$ = molar concentration of gas A at the surface of the particle
C_B = molar density of solid reactant B
C_C = molar density of solid product C
C^i = integration constants for i's species
C_p = molar concentration of p within the macropores
C_p^o = interfacial molar concentration of p
C_S^∞ = initial concentration of S
D_{eM} = binary molecular diffusivity of an electrolyte
D_{gM} = binary molecular diffusivity of a gas
$\bar{D}_P$ = average particle size
$\bar{D}_r$ = average pore diameter
D'_{pea} = effective diffusivity of p in the ash layer
D_{pb} = bulk diffusivity of p
D_{pe} = effective diffusivity of p
$\bar{D}_{pe}$ = dimensionless effective diffusivity of p, D_{pe}/D_{pb}
D'_{pbf} = bulk diffusivity of p in the liquid film
D_{pM} = molecular diffusivity of p
F = Faraday's constant
G_p = dimensionless molar concentration of p, $C_p/C_{A\infty}$
$G_{S\infty}$ = dimensionless initial concentration of S, $C_S^\infty/C_{A\infty}$
h'' = stoichiometric coefficient equaling 1
H = ionic reactant and product
I = ionic strength
K_{sp} = equilibrium constant for Eq. 2
M = molecular weight
n_M = valence of species M
q = stoichiometric coefficient equaling 1
q' = stoichiometric coefficient equaling 14
q'' = stoichiometric coefficient equaling 14
Q_o = oxidized state of Q

Q_r = reduced state of Q
r = macroscopic radial distance in spherical coordinate
r' = microscopic radial distance in spherical coordinate
r^* = initial grain radius
r_c = radius of unreacted core
r_o = radius of shrinking ash
R = gas constant
R_o = radius of particle
s = stoichiometric coefficient equaling 1
s' = stoichiometric coefficient equaling 1
$\bar{s}$ = stoichiometric coefficient equaling 1
S = ionic product
t = time
T = absolute temperature
V = dimensionless ash-layer radius, r_o/r^*
V_g = molecular volume of a gas at its normal boiling point
w_o = initial weight fraction of reactant solid B
x = local conversion of reactant solid B
X = overall conversion of reactant solid B
Y = dimensionless core radius, r_c/r^*
Z = dimensionless macroscopic radial coordinate, r/R_o
Z_g^* = dimensionless macroscopic moving boundary of grains
Z_P = charge of species P

Greek letters

α'_{AQo} = dimensionless diffusivity, Eq. 20 or 23, D'_{Abf}/D'_{Qobf}
α'_p = dimensionless diffusivity of p, D'_{pbf}/D'_{Qobf}
β = ratio of initial grain radius to liquid film thickness, r^*/δ
γ_j = number of moles of j in one mole of C
Γ_g = time required for complete conversion of the grains at the surface
φ = quantity defined in Eq. 5, $3w_o\rho_{bo}R_o^2/\rho_B r^{*2}$
δ = thickness of liquid film
δ_b = thickness of bacterial film
Δ = relative effective diffusivity of ferrous to ferric, D_{Qre}/D_{Qoe}
ϵ = porosity of particle
ϵ' = porosity of ash layer
ϵ_o = initial porosity of particle
η_p = dimensionless diffusivity of p, D'_{pbf}/D'_{peq}
θ_p = quantity defined in Eq. 11 or 15, D_{pb}/R_o^2
λ_M^o = limiting ionic conductance of M
λ_p = quantity defined in Eq. 22 or 23, $D'_{Qobf}C_{A\infty}/r^{*2}C_C\gamma_p$
μ = viscosity of solution
ξ_p^o = dimensionless molar concentration of p at the surface of the solid, $C_p^o/C_{A\infty}$
π_p = dimensionless diffusivity of p, D_{pb}/D'_{pbf}
ρ_{bo} = initial bulk density of particle
ρ_B = density of reactant solid B
σ = quantity defined in Eq. 20, $\bar{b}_A D'_{Abf}C_{A\infty}/r^{*2}C_B$
τ = tortuosity factor of pores within particle
τ' = tortuosity factor of ash layer
ϕ = association factor
ψ = quantity defined in Eq. 19, $r^{*2}/3\ R_o^2$
$\omega_{\bar{b}}$ = ratio of stoichiometric coefficients equaling 1/4
ω_q = ratio of stoichiometric coefficients equaling 1
ω_{sa} = ratio of stoichiometric coefficients equaling 2/7
$\omega_{s'q'}$ = ratio of stoichiometric coefficients equaling 1/4
Ω = quantity defined in Eq. 25, $\bar{K}_{sp}C_{A\infty}^{h''-q-\bar{s}}$

Subscripts

a = refers to ash layer
g = refers to grain
Ig = refers to region I where $Y=0$
IIg = refers to region II where $Y\neq 0$
i = refers to A or Q_o
j = refers to Q_r or S
p = refers to A, Q_Q, Q_r, S, or H
P = refers to ionic species only

Literature Cited

Batarseh, K. I., "Mathematical Modeling on the Role of *Thiobacillus Ferrooxidans* in the Formation of Acid Mine Drainage," PhD Diss., Dept. of Chemical Engineering, West Virginia Univ. (1992).

Batarseh, K. I., G. P. Swaney, and A. H. Stiller, "A Mathematical Model for Heterogeneous Reactions with a Moving Boundary," *AIChE J.*, **35**, 625 (1989).

Batarseh, K. I., "The Effect of Physical Properties of Toxic Mine Waste on Acid Mine Drainage: A Mathematical Model," MS Thesis, Dept. of Chemical Engineering, West Virginia Univ. (1987).

Bhatia, S. K., "Perturbation Analysis of Gas-Solid Reactions," *Chem. Eng. Sci.*, **46**, 173 (1991).

Bhatia, S. K., "Analysis of Distributed Pore Closure in Gas-Solid Reactions," *AIChE J.*, **31**, 642 (1985).

Bhatia, S. K., and D. D. Perlmutter, "A Random Pore Model for Fluid-Solid Reactions: II. Diffusion and Transport Effects," *AIChE J.*, **27**, 247 (1981).

Bhatia, S. K., and D. D. Perlmutter, "A Random Pore Model for Fluid-Solid Reactions: I. Isothermal, Kinetic Control," *AIChE J.*, **26**, 379 (1980).

Bischoff, K. B., "Further Comments on the Pseudo-Steady State Approximation for Moving Boundary Diffusion Problems," *Chem. Eng. Sci.*, **20**, 783 (1965).

Bischoff, K. B., "Accuracy of the Pseudo Steady State Approximation for Moving Boundary Diffusion Problems," *Chem. Eng. Sci.*, **18**, 711 (1963).

Blancarte-Zurita, M. A., R. M. R. Branion, and R. W. Lawrence, "Particle Size Effects in the Microbial Leaching of Sulfide Concentrates by Thiobacillus Ferrooxidans," *Biotechnol. Bioeng.*, **28**, 751 (1986).

Bowen, J. R., "Comments on the Pseudo-Steady State Approximation for Moving Boundary Problems," *Chem. Eng. Sci.*, **20**, 712 (1965).

Brierley, L. C., "Bacterial Leaching," *CRC Crit. Rev. Microbiol.*, **5**, 207 (1978).

Brown, L. F., H. W. Haynes, and W. H. Manogue, "The Prediction of Diffusion Rates in Porous Materials at Different Pressures," *J. Catal.*, **14**, 220 (1969).

Carslaw, H. J., and J. C. Jäger, *Conduction of Heat in Solids*, Clarendon Press, Oxford (1959).

Cathles, L. M., and J. A. Apps, "A Model of the Dump Leaching Process that Incorporates Oxygen Balance, Heat Balance, and Air Convection," *Met. Trans.*, **6B**, 617 (1975).

Colmer, A. R., and M. E. Hinkle, "The Role of Microorganisms in Acid Mine Drainage," *Sci.*, **106**, 253 (1947).

Crank, J., *The Mathematics of Diffusion*, Oxford, London (1975).

Cussler, E. L., J. Kopinsky, and J. A. Weimer, "Effect of Pore Diffusion on the Dissolution of Porous Mixtures," *Chem. Eng. Sci.*, **38**, 2027 (1983).

Cussler, E. L., "Dissolution and Reprecipitation of Porous Solids," *AIChE J.*, **28**, 500 (1982).

Cussler, E. L., and J. D. B. Featherstone, "Demineralization of Porous Solids," *Sci.*, **213**, 1018 (1981).

Dassori, C. G., J. W. Tierney, and Y. T. Shah, "A Gas-Solid Reaction with Nonuniform Distribution of Solid Reactant," *AIChE J.*, **34**, 1878 (1988).

Delikouras, E. A., and D. D. Perlmutter, "Combined Effects of Mass Transfer and Inaccessible Porosity in Gasification Reactions," *AIChE J.*, **39**, 829 (1993).

Dutrizac, S. E., and R. J. C. MacDonald, "Ferric Ion as a Leaching Medium" *Miner. Sci. Eng.*, **6**, 59 (1974).

Ehrlich, H. L., and S. I. Fox, "Environmental Effects on Bacterial Copper Extraction from Low-Grade Copper Sulfide Ores," *Biotechnol. Bioeng.*, **9**, 471 (1967).

Fortini, A. J., and D. D. Perlmutter, "Porosity Effects in Hydrogen Reduction of Iron Oxides," *AIChE J.*, **35**, 1245 (1989).

Gerogakis, C., D. W. Chang, and J. Szekely, "A Changing Grain Size Model for Gas-Solid Reactions," *Chem. Eng. Sci.*, **34**, 72 (1979).

Ingledew, W. J., "Thiobacillus Ferrooxidans—The Bioenergetic of an Acidophilic Chemolithotroph," *Biochim. Biophys. Acta*, **683**, 89 (1982).

Ingledew, W. J., J. C. Cox, and P. J. Helling, "A Proposed Mechanism for Energy Conservation During Iron (II) Oxidation by Thio-

bacillus Ferrooxidans: Chemiosmotic Coupling to Net Proton Influx," *Proc. Soc. Gen. Microbiol*, **4**, 74 (1977).
Kargi, F., "Mathematical Model for Microbial Oxidation of Pure Lead Sulfide by Thiobacillus Ferrooxidans," *Biotechnol. Bioeng.*, **34**, 487 (1989).
Kelly, D. P., P. R. Morris, and C. L. Brierley, in *Microbiol. Technology Current State Future Prospects*, A. T. Bull, D. C. Ellwood, and C. Ratledge, eds., Cambridge University Press (1979).
Kopinsky, J., R. Aris, and E. L. Cussler, "Theories of Precipitation Induced by Dissolution," *AIChE J.*, **34**, 2005 (1988).
Krishnamurthy, S., and Y. T. Shah, "An Approximate Solution to the Moving Boundary Problem with Two Simultaneous Reactions," *Chem. Eng. Sci.*, **34**, 1967 (1979).
Lacey, D. T., and F. Lawson, "Kinetics of the Liquid-Phase Oxidation of Acid Ferrous Sulfate by the Bacterium Thiobacillus Ferrooxidans," *Biotechnol. Bioeng.*, **12**, 29 (1970).
Lichtner, P. C., E. H. Oelkers, and H. C. Helgeson, "Exact and Numerical Solutions to the Moving Boundary Problem Resulting from Reversible Heterogeneous Reactions and Aqueous Diffusion in a Porous Medium," *J. Geophys. Res.*, **B91:7**, 7531 (1986a).
Lichtner, P. C., E. H. Oelkers, and H. C. Helgeson, "Interdiffusion with Multiple Precipitation/Dissolution Reactions: Transient Model and the Steady-State Limit," *Geochim. et Cosmochim. Acta*, **50**, 1951 (1986b).
McCabe, W. L., and J. C. Smith, *Unit Operations of Chemical Engineering*, 3rd ed., McGraw-Hill, New York (1976).
Meredith, R. E., and C. W. Tobias, "II. Conduction in Heterogeneous Systems," *Adv. Electrochem. Electrochem. Eng.*, **2**, 15 (1962).
Morell, J. I., and N. R. Amundson, "The Combustion Behavior of Retorted Shale Particles," *Chem. Eng. Sci.*, **45**, 3247 (1990).
Murr, L. E., "Theory and Practice of Copper Sulphide Leaching in Dumps and In-Situ," *Miner. Sci. Eng.*, **12**, 121 (1980).
Novak, C. F., R. S. Schechter, and L. W. Lake, "Diffusion and Solid Dissolution/Precipitation in Permeable Media," *AIChE J.*, **35**, 1057 (1989).
Perry, J. H., and C. H. Chilton, *Chemical Engineers' Handbook*, McGraw-Hill, New York (1973).
Pinches, A., F. O. Al-Jaid, D. J. A. William, and B. Atkinson, "Leaching of Chalcopyrite Concentrates with Thiobacillus Ferrooxidans in Batch Culture," *Hydrometal.*, **2**, 87 (1976).
Prasannan, P. C., P. A. Ramachandran, and L. K. Doraiswamy, "A Model for Gas-Solid Reactions with Structural Changes in the Presence of Inert Solids," *Chem. Eng. Sci.*, **40**, 1251 (1985).
Ramachandran, P. A., and J. M. Smith, "Effect of Sintering and Porosity Changes on the Rate of Gas-Solid Reactions," *Chem. Eng. J.*, **14**, 137 (1977a).
Ramachandran, P. A., and J. M. Smith, "A Single-Pore Model for Gas-Solid Noncatalytic Reactions," *AIChE J.*, **23**, 353 (1977b).
Ranade, P. V., and D. P. Harrison, "The Grain Model Applied to Porous Solids with Varying Structural Properties," *Chem. Eng. Sci.*, **34**, 427 (1979).
Reid, C. R., J. M. Prausnitz, and T. K. Sherwood, *The Properties of Gases and Liquids*, 3rd ed., McGraw-Hill, New York (1977).
Renton, J. J., A. H. Stiller, and T. Rymer, "A Laboratory Procedure to Evaluate the Acid Producing Potential of Coal Associated Rocks," *Annual Surface Mine Drainage Reclamation Assoc. Symp.*, West Virginia Univ. (1984).
Robinson, R. A., and R. H. Stokes, *Electrolyte Solutions*, Butterworths, London (1959).
Satterfield, C. N., *Mass Transfer in Heterogeneous Catalysis*, MIT Press (1970).
Silverman, M. P., M. H. Rogoff, and I. Wender, "Bacterial Oxidation of Pyrite Materials in Coal," *Appl. Microbiol.*, **9**, 491 (1961).
Silverman, M. P., and D. G. Lundgren, "An Improved Medium and a Harvesting Procedure for Securing High Cell Yields," *J. Bact.*, **77**, 642 (1958).
Singer, P. C., and W. Stumm, "Acid Mine Drainage: The Rate Determining Step," *Sci.*, **167**, 1121 (1970).
Sotirchos, S. V., and N. R. Amundson, "Dynamic Behavior of a Porous Char Particle Burning in an Oxygen Containing Environment: 1. Constant Radius Particle," *AIChE J.*, **30**, 537 (1984a).
Sotirchos, S. V., and N. R. Amundson, "Dynamic Behavior of a Porous Char Particle Burning in an Oxygen Containing Environment: 2. Transient Analysis of a Shrinking Particle," *AIChE J.*, **30**, 549 (1984b).
Szekely, J., C. I. Lin, and H. Y. Sohn, "A Structural Model for Gas-Solid Reactions with a Moving Boundary: V. An Experimental Study of the Reduction of Porous Nickel-Oxide Pellets with Hydrogen," *Chem. Eng. Sci.*, **28**, 1975 (1973).
Szekely, J., and J. W. Evans, "A Structural Model for Gas-Solid Reactions with a Moving Boundary: I," *Chem. Eng. Sci.*, **25**, 1091 (1969).
Szekely, J., and J. W. Evans, "A Structural Model for Gas-Solid Reactions with a Moving Boundary: II," *Chem. Eng. Sci.*, **26**, 1901 (1971).
Theofanous, T. G., and H. C. Lim, "An Approximate Analytical Solution for Non-planar Moving Boundary Problems," *Chem. Eng. Sci.*, **26**, 1297 (1971).
Torma, A. E., *Adv. Biochem. Eng.*, T. K. Ghose, A. Frechter, and N. Blackebrough, eds., **6**, 1 (1977).
Torma, A. E., and R. Guay, "Effect of Particle Size on the Biodegradation of a Sphalerite Concentrate," *Nat. Can.*, **103**, 133 (1976).
Tsaur, K., and R. Pollard, "Mathematical Modeling of the Lithium, Thionyl Chloride Static Cell: I. Neutral Electrolyte," *J. Electrochem. Soc.*, **131**, 975 (1984a).
Tsaur, K., and R. Pollard, "Mathematical Modeling of the Lithium, Thionyl Chloride Static Cell: II. Acid Electrolyte," *J. Electrochem. Soc.*, **131**, 984 (1984b).
Wakao, N., and J. M. Smith, "Diffusion in Catalyst Pellets," *Chem. Eng. Sci.*, **17**, 825 (1962).
Wilke, C. R., and P. Change, "Correlation of Diffusion Coefficients in Dilute Solutions," *AIChE J.*, **1**, 264 (1955).

Appendix: Parameter Evaluation

To be able to predict quantitatively the reaction of pyrite, numerical values for the transport and thermodynamic properties pertaining to this system must be determined. In addition, the model has three adjustable parameters which must be determined, namely, the thickness of the liquid film surrounding the grains, δ, the porosity, ϵ', and tortuosity factor, τ', of the ash layer. Most of these data can be readily obtained either theoretically or experimentally from information found in the literature. In this segment, we will give a synopsis regarding the evaluation of these constants. One may wonder about the reasons behind it, and there is no doubt that some will foresee this as *deja vu*. Nonetheless, from the practical side, there is again a confusion which manifests itself as a failure to distinguish between the different correlations presented in the literature and their applications which very often can be misleading. The purpose of this synopsis is not to inflate on this subject, but simply to provide the principal equations and methods needed for the theoretical predictions.

Effective diffusion coefficient

In general, the effective diffusion coefficient D_{pe} in a porous medium will vary with the structural parameters of the solid according to:

$$D_{pe} = \epsilon D_{pM}/\tau(\epsilon) \tag{A1}$$

where D_{pM} is the molecular diffusivity of p, and ϵ and τ are the porosity and tortuosity factor of the solid, respectively. Obviously, the above expression neglects Knudsen diffusion in the porous system since the transport occurs in a liquid medium. Equation A1 suggests that the tortuosity factor varies with porosity.

In accounting for the variations in effective diffusivity with the progress of reactions, the model of Wakao and Smith (1962) was used in this work. Hence,

$$\tau = 1/\epsilon \qquad \text{(A2)}$$

In electrochemical systems, for example, the tortuosity factor is commonly represented by $\tau = 1/\epsilon^{1/2}$ (Meredith and Tobias, 1962; Tsaur and Pollard, 1984a,b). The Wakao and Smith model has been experimentally verified (Brown et al., 1969), and has been widely used in chemical engineering to describe the variations of τ with conversion for similar problems (for example, Ranade and Harrison, 1979; Bhatia and Perlmutter, 1981; Sotirchos and Amundson, 1984a,b; Morell and Amundson, 1990; Delikouras and Perlmutter, 1993). Ranade and Harrison (1979), for instance, have used this model to extend the grain model to account for structural changes. It is noteworthy to mention that the tortuosity factor cannot be taken constant in this work due to the simultaneous dissolution and precipitation of ferrous sulfate occurring in different regions of the particle which result in variations of the porous structure (see Table 3). Further along these lines, a constant tortuosity factor becomes meaningless once precipitation is the norm where the pores gradually constrict along their length and eventually close. Consequently, diffusion in this vicinity will be progressively inhibited, and then completely stopped.

The binary molecular diffusivities of the gaseous species, D_{gM}, and of the electrolyte species, D_{eM}, can be estimated from the Wilke-Change (1955), and the Nernst-Haskell (Reid et al., 1977) formulas:

$$D_{gM} = 7.4 \times 10^{-8} T(\phi M)^{0.5}/\mu V_g^{0.6} \quad (\text{cm}^2/\text{s}) \text{ and} \qquad \text{(A3)}$$

$$D_{eM} = RT\lambda_M^o/|n_M|F^2 \quad (\text{cm}^2/\text{s}) \qquad \text{(A4)}$$

with the approximate guide to temperature dependence

$$D_{eM}\mu/T = \text{constant} \qquad \text{(A5)}$$

The values for ϕ, μ, V_g, and λ_M^o can be obtained from published data.

To compute the macroeffective diffusivity within the pores of the particles, D_{pe}, only the dependence of the porosity on the rate of shrinking of the ash layer is needed. This functionality for this model is given by Eq. 19 in which the initial porosity, ϵ_o, can be determined from mercury porosimetry experiments. Calculating the microeffective diffusivity, on the other hand, is straightforward provided that ferrous sulfate porosity ϵ' and tortuosity factor τ'—taken to be constants—are known. Since these structural parameters are difficult to obtain in practice, numerical values must be assigned. Since the product of the reaction, szomolnokite, is the same in this case and in our previous article (Batarseh et al., 1989), the values of ϵ' and τ' of the ash layer were taken from this cited article.

Equilibrium constant

Equation 25 embodies a constant, namely: the solubility product $\overline{K}_{sp}$. This constant for ferrous sulfate can be readily determined for solubility experiments provided an expression for the activity coefficients is available. In this work we used the equation given by Guggenheim (Robinson and Stokes, 1959):

$$\ln a_P = -\frac{1.178\ |Z_P|\ \sqrt{I}}{1+\sqrt{I}} + 0.1\ |Z_P| I \qquad \text{(A6)}$$

where a_P is the activity coefficient of Pth ionic species and Z_P is its charge, and I is the ionic strength of the solution which equals to $1/2\ \Sigma_P Z_P^2 C_P$ (C_P is the concentration of Pth species).

Liquid film thickness

Needed in the theoretical predictions is a numerical value for δ (the liquid film thickness surrounding the ash layer). It is a property which depends on the diameter of the grain. The magnitude of this parameter cannot be readily determined. Therefore, in a similar fashion to that of ϵ' and τ', its value was deduced by fitting the calculated conversion profiles to the ones obtained experimentally, and the value of this parameter which minimized the error between calculated and observed was chosen. The value obtained for δ by this procedure was checked against mutual values presented in the literature as a confirmation for the reliability of its magnitude. In the published literature, a diffusion in a stagnant film will typically have a Sherwood Number of about 2.0 (McCabe and Smith, 1976). Thus, it is expected that δ would be in the order of one-half of the diameter of the grain. *It should be noted that the same values of these adjustable parameters, δ, ϵ', and τ', were used throughout the theoretical predictions regardless of experimental conditions.*

Manuscript received July 9, 1993, and revision received Nov. 2, 1993.